



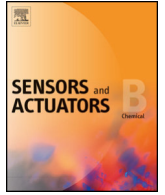
<b>Publication Year</b>	2016
<b>Acceptance in OA</b>	2020-05-27T08:45:12Z
<b>Title</b>	Photosensitive chipless radio-frequency tag for low-cost monitoring of light-sensitive goods
<b>Authors</b>	Oliveros, M., Carminati, M., ZANUTTA, Alessio, Mattila, T., Jussila, S., Nummila, K., BIANCO, ANDREA, Lanzani, G., Caironi, M.
<b>Publisher's version (DOI)</b>	10.1016/j.snb.2015.09.144
<b>Handle</b>	<a href="http://hdl.handle.net/20.500.12386/25208">http://hdl.handle.net/20.500.12386/25208</a>
<b>Journal</b>	SENSORS AND ACTUATORS. B, CHEMICAL
<b>Volume</b>	223



Contents lists available at ScienceDirect

## Sensors and Actuators B: Chemical

journal homepage: [www.elsevier.com/locate/snb](http://www.elsevier.com/locate/snb)



# 1 Photosensitive chipless radio-frequency tag for low-cost monitoring 2 of light-sensitive goods

3 **Q1** M. Oliveros<sup>a,b</sup>, M. Carminati<sup>c</sup>, A. Zanutta<sup>d</sup>, T. Mattila<sup>e</sup>, S. Jussila<sup>e</sup>, K. Nummila<sup>e</sup>,  
4 A. Bianco<sup>d</sup>, G. Lanzani<sup>a,b</sup>, M. Caironi<sup>a,\*</sup>

5 <sup>a</sup> Center for Nano Science and Technology @PoliMi, Istituto Italiano di Tecnologia, Milano, Italy

6 <sup>b</sup> Dipartimento di Fisica, Politecnico di Milano, Milano, Italy

7 <sup>c</sup> Dipartimento di Elettronica, Informazione e Bioingegneria, Politecnico di Milano, Milano, Italy

8 <sup>d</sup> INAF – Osservatorio Astronomico di Brera, Merate, Italy

9 <sup>e</sup> VTT Technical Research Centre of Finland Ltd, Espoo, Finland

### 16 A R T I C L E I N F O

#### 12 Article history:

13 Received 11 February 2015

14 Received in revised form

15 25 September 2015

16 Accepted 28 September 2015

17 Available online xxx

#### 19 Keywords:

20 RFID

21 Sensor chipless tag

22 Wireless sensor

23 Light exposure detector

24 Photopolymer

### A B S T R A C T

A simple approach to develop a novel photosensitive RF tag to be used as non-volatile wireless light exposure detector is presented. This chipless tag is based on the coupling of a standard HF LC resonator with an interdigitated planar sensor featuring a micrometric inter-electrode gap optimized for a thin acrylamide photosensitive polymer layer. Exposure to ambient light within the absorbance band of the photosensitizer (~530 nm) triggers polymerization, which irreversibly modifies the electrical properties of the film, producing a significant decrease of the dielectric constant of 27%, thereby changing the resonance frequency (540 kHz shift) of the resonator. This allows the straightforward wireless detection of the light exposure event as demonstrated here. The sensor fabrication is fully compatible with high-throughput printing processes, therefore fostering a dramatic reduction of tag production costs and enabling mass application of disposable tags that can, for instance, be embedded into the packaging of light-sensitive goods.

© 2015 Published by Elsevier B.V.

## 27 1. Introduction

28 **Q3** Radio frequency identification (RFID) is a wireless data capturing  
29 technique which utilizes radio frequency (RF) waves for the  
30 purposes of contact-less identification, monitoring and authentication  
31 of objects. RFID relies on RF waves for data transmission  
32 between the data carrying device (the RFID tag) and the interrogator  
33 (RFID reader) [1]. Today, the growing tendency in supply chain  
34 management and goods handling is to replace barcodes with RFID  
35 transponders, which have unique ID codes for individual items that  
36 can be automatically read at a longer distance [2]. The reason why  
37 RFID tags have not yet overtaken barcodes is partly the cost of the  
38 tag, being still much higher for an RFID tag than for a simple barcode  
39 label [3]. RFID technology has in any case been successfully

40 applied in the areas of manufacturing, supply chains, agriculture,  
41 transportation, and healthcare to name a few [4].

42 Tags can be passive (powered by RF radiation of the reader) or  
43 active (including a power source such as a battery or an energy  
44 harvesting device). They can be read only or read/write. Typically,  
45 passive tags are smaller, lighter and simpler than active ones, and  
46 noticeably less expensive. They are maintenance-free and have an  
47 almost indefinite operating life. In order to significantly reduce the  
48 cost per tag, chipless RFID tags [5], where no active electronics  
49 is present, are being developed. A chipless RF tag for high frequencies  
50 (HF) can be implemented, for example, as a LC-resonator, where  
51 typically a planar coil is connected to a capacitor. The simplicity of  
52 the system comes at the cost of functionality, which is usually limited  
53 to the detection of the presence or the absence of the resonator (by  
54 looking at the presence of the resonance), as widely used in anti-theft  
55 tags [6]. Research on chipless RFID tags has been recently focusing on  
56 the integration of sensing capabilities within the tags, thus greatly  
57 extending their applications. Sensing is achieved by introducing  
58 materials which are sensitive to specific external stimuli, thereby  
59 affecting the impedance of the tag. These

\* Corresponding author at: Center for Nano Science and Technology @PoliMi, Istituto Italiano di Tecnologia, Via Pascoli, 70/3, 20133 Milano, Italy.  
E-mail address: [mario.caironi@iit.it](mailto:mario.caironi@iit.it) (M. Caironi).

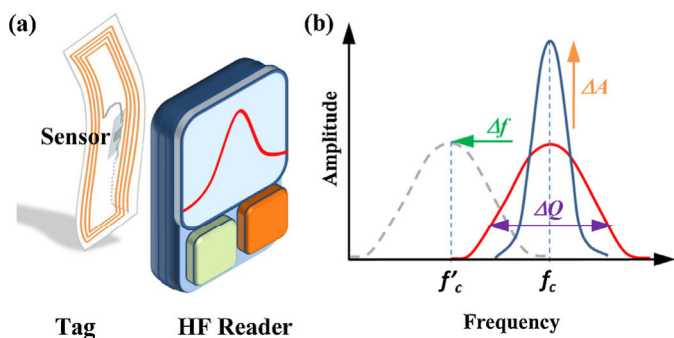


**Fig. 1.** Working principle of a chipless tag: (a) RF interrogation to detect the (b) alteration of the resonance features (resonance frequency  $f_c$ , amplitude  $A$  or quality factor  $Q$ ) induced by an impedance modification of the sensor embedded in the tag and exposed to a chemo-physical stimulus.

changes in inductance, capacitance or dissipation can be detected by measuring the resonance frequency  $f_c$  and the quality factor  $Q$  of the tag. The general working principle and the detection approach for chipless HF tag sensors are described in Fig. 1.

Several examples of wireless sensors that use the passive resonator approach have been proposed in the literature for the detection of pressure [7], toxic [8] and non-toxic [9] gases, humidity [10,11], hazardous compounds in water systems [12], chemical sensing [13] based on graphene/silk sensors for bacteria detection and biochemical sensors [14] based on the combination of the capacitive pressure sensing technique and biosensitive hydrogels [15] and pH [16].

So far, there has not been any report on the possibility of developing a light-sensitive chipless tag following the very simple approach of fabricating a planar photosensitive resonator, while such a wireless sensor would be of particular interest for tagging of goods which must not be exposed to light. The possible exposure to light could be then certified with a simple and fast wireless measurement, without the need to interfere with the goods or to open the package. The result can be stored as a simple, single-bit information, which can subsequently reveal whether exposure has occurred or not, as a sort of wireless “litmus test”. Such application may have a strong impact on the food or pharmaceutical industry or, in any case, where exposition to light must be avoided or certified.

In this paper we report on a photosensitive, chipless RFID plastic tag where an LC resonator is coupled with a photopolymer-based microsensors contributing to the tag capacitance. The photopolymer layer provides the photosensitivity in the green spectral region and, upon light exposure an irreversible polymerization takes place, resulting in an irreversible change in its dielectric constant that can be measured. This process allows for a permanent record of a light

exposure event through the effects on the electric properties of the RFID tag.

## 2. Materials and methods

### 2.1. Photopolymer formulation

The precursor formulation of the photopolymer adopted in this study has been prepared following the system developed by Sugawara et al. [17]. It consists of acrylamide as monomer, a cross-linker (N,N'-methylene bis-acrylamide), a sensitizer (Erythrosin B), and an electron donor (triethanolamine, TEA). Additionally Polyvinylalcohol (PVA) is added as a binder, to allow the production of dry photopolymer layers (Fig. 2(c)).

The light is absorbed by the sensitizer, which then reacts with the electron donor, providing free radicals that start the polymerization of acrylamide monomers. During the polymerization, the viscosity of the medium increases and the reaction slows down. The radical polymerization stops through the usual mechanisms (combination of two active chain ends, combination of an active chain end with an initiator radical). Details of the photoreaction can be found in the work by Lawrence and co-workers [18]. The dye (Erythrosin B) shows a maximum absorbance peak at 526 nm, providing a sensitivity range from 500 nm to 550 nm. Interestingly, by changing the dye structure and/or mixing different dyes it is possible to tune the sensitivity of the photopolymer in the visible band [19] and also to have a panchromatic system [20].

The photopolymer formulation was prepared by adding 1 g of PVA (to be stored in dark) to 10 ml of bi-deionized water. The solution was heated at 90 °C and stirred until complete PVA dissolution. Successively 0.24 g of acrylamide, 0.08 g of bis-acrylamide, 0.8 ml of TEA and 1.6 ml ( $1.76 \cdot 10^{-4}$  g/ml) of Erythrosin B were added to 7 ml of PVA solution. The formulation was prepared at room temperature in normal light conditions and stored in dark conditions at room temperature for no more than 2 days before use.

### 2.2. Tag fabrication

The tag developed in this work is based on a commercially available, standard anti-theft tag (EAS – Electronic Article Surveillance) consisting of a coil, a capacitor and a fuse on a plastic foil. The tag has been modified by removing the fuse which normally connects the coil to the top and bottom plates of the capacitor. After the removal of the capacitor bottom plate, the characteristic resonance frequency  $f_c$  changes from the original value of 8.5 MHz–30 MHz. The interdigitated sensor was attached on a free area in the middle of the tag and the electrodes were connected to the coil terminals by means of silver paste. The resonance frequency of the fully

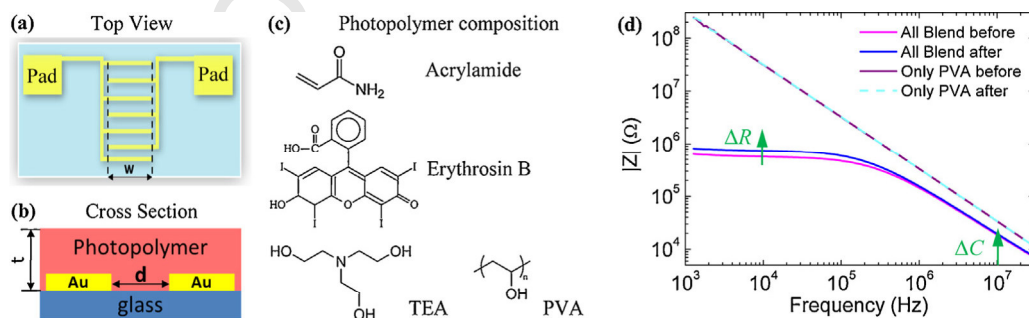


**Fig. 2.** The sensors are fabricated with standard lithography: (a) top view and (b) cross section of the interdigitated gold microelectrodes covered with a photopolymer film (c) of thickness  $t$ . (d) Magnitude of the impedance spectra of a test device ( $t = 1.6 \mu\text{m}$ ,  $d = 5 \mu\text{m}$ ,  $l = W-20$  fingers = 1 cm) before (magenta line) and after (blue line) the polymerization process. For comparison, the impedance of a film containing only PVA, showing a pure capacitive behavior, both before (violet line) and after exposure (cyan dashed line), is also reported. (For interpretation of the references to color in this figure legend, the reader is referred to the web version of this article.)

assembled tag is ~13 MHz, chosen to be in the same range as the widespread standard of HF RFID tags operating at 13.56 MHz.

### 2.3. Interdigitated sensors

The sensors consist of interdigitated 45 nm-thick Au electrodes, fabricated by a two-step lift-off photolithographic process on top of a Corning 1737F substrate and coated with a layer of the photopolymer (Fig. 2(a)). The gap between the fingers ( $d$ ), indicated in the following as channel length, varies from 5  $\mu\text{m}$  to 40  $\mu\text{m}$ , and the total length of the fingers ( $\ell$ ) is either 1 or 2.5 cm. The precursor formulation, filtered with a 5  $\mu\text{m}$  nylon filter, is deposited on top of the electrodes by spin-coating. Different photopolymer thicknesses ( $t$ ), from 500 nm to 20  $\mu\text{m}$ , can be obtained by varying the spin speed from 1500 r.p.m. to 200 r.p.m. The results here reported refer to 1.6  $\mu\text{m}$  and 20.5  $\mu\text{m}$  thicknesses. Finally, the thickest film (~100  $\mu\text{m}$ ) is instead deposited by drop-casting. All the fabrication steps were performed in a nitrogen glove box and using a red light to fabricate the devices.

### 2.4. Electrical measurements

Impedance spectroscopy measurements were performed in a nitrogen glove box with a two point contact setup, by applying a 500 mV sine wave in the 40 Hz–110 MHz wide frequency range with an Agilent 4294A Impedance Analyzer. Impedance measurements before photopolymerization were performed using a red light and at room temperature.

Measurements of the complete tags were performed by employing a reader antenna connected to an Agilent E5061B ENA Network Analyzer to extract the scattering parameters. The reader antenna is made of two loops, which are inductively coupled. The mutual inductive coupling between the reader antenna and the tag enables a contactless detection of the tag parameters of interest. The reader antenna and the tag have been placed parallel to each other at a distance of 1 cm in all the reported measurements. Measurements of the tags before light exposure have been performed in darkness using a special black box that completely covers the antenna and the reader.

## 3. Results and discussion

Our strategy for the development of a photosensitive chipless RF tag was to couple a sensor, based on a suitable active medium, with a LC resonator. Light exposure modifies the electrical parameters of the sensor, i.e. its impedance, and therefore induces changes in the measurable tag parameters, such as  $f_C$  and  $Q$ . In order to develop a photosensitive tag, we tested the possibility to induce a variation in the dielectric constant of an acrylamide photopolymer film (described in Section 2.1) at frequencies compatible with integration in a wireless sensor. It is well known that films based on such acrylamide-based photopolymers can undergo a variation in the refractive index upon light exposure [21], and for this reason they are largely adopted for volume holography. A change in the refractive index represents a variation of the relative dielectric constant at optical frequencies. To the best of our knowledge, the effects of an exposure to ambient light on the dielectric constant of acrylamide photopolymers at MHz frequencies have not been previously investigated.

Our approach, detailed in the following sections, is here summarized. (i) We validate the use of a photo-polymer, with a thickness ( $t$ ) of 1.6  $\mu\text{m}$ , a common thickness adopted for other optoelectronic applications [17–20], to develop the sensing functionality; (ii) we verify that, even in the suboptimal case of electrodes spaced by 5  $\mu\text{m}$ , limited by the available lithographic patterns, a change in the impedance spectrum is apparent, both as a variation in resistance

and capacitance; (iii) we select the capacitive sensing approach, preferred to the resistive one, since it allows for easier detection (a frequency shift rather than a quality factor change in the frequency range of the tag resonance); (iv) we use a set of different electrodes, spaced from 5  $\mu\text{m}$  to 40  $\mu\text{m}$ , to assess the change in the material dielectric constant by means of *conformal mapping*-based numerical simulations, and we use this result to fit experimental data and to obtain the maximum achievable capacitance variation with any geometry; on the basis of the rationale obtained in the previous points (v) we design an operative device, choosing the optimal deposition thickness (>20  $\mu\text{m}$ ) for the 5  $\mu\text{m}$  spaced electrodes, and (vi) we couple it to a commercial RF coil for the experimental contactless validation of the full sensor.

### 3.1. Preliminary impedance characterization of interdigitated sensors

The photopolymer-based sensors have been characterized by measuring their impedance as a function of frequency before and after the photopolymerization process. Due to the high sensitivity of the material to light, we took special care in fabricating all samples under a red light, which does not trigger polymerization as it is not absorbed by the sensitizer. This is also the condition that we adopted to measure the impedance of the sensors before polymerization. When the film is irradiated with ambient light, the polymerization takes place as previously described. Visibly, the color of the film during the polymerization fades, and the film passes from being clearly red to transparent due to consumption of the dye. Correspondingly, the electrical properties of the film change.

The initial test device, used to assess photosensitivity, is coated with a 1.6  $\mu\text{m}$  thick layer of photopolymer. Consequently, we chose electrodes with relatively small gaps ( $d = 5 \mu\text{m}$ ,  $\ell = 1 \text{ cm}$ ). The Bode plots of the magnitude of the measured impedance spectra before and after the exposure of the device to a 526 nm radiation (intensity ~10  $\mu\text{W}/\text{cm}^2$ ) for 20 min are reported in Fig. 2(d). Neglecting the contact impedance that is dominant at very low frequency, the sensor impedance can be approximately modeled with a simple  $R||C$  parallel circuit, the parameters of which are characteristic of the photopolymer formulation and cannot be observed with the single components. PVA for example, which enables the filming of the material, provides a pure capacitive behavior on the (Fig. 2(d)) with no measurable difference in the value of capacitance before (continuous violet line) and after exposure (dashed cyan line). Among the various components of the precursor formulation, we identify the specific role of the electron donor TEA in determining the resistive behavior between 1 kHz and ~100 kHz. This can be ascribed to the electron donor properties of the amine, which could increase the transport properties of holes through the film. This explanation is supported by the observation that triarylamines have been widely used in xerography process as a dopant in polymer films (especially polystyrene) to improve the holes transportation [22]. Below 1 kHz the impedance increases with lower frequencies and follows a capacitive behavior, indicating the presence of a blocking interface.

In initial dark conditions (pink spectrum)  $R$  (measured at 10 kHz) is equal to 592 k $\Omega$  and  $C = 0.97 \text{ pF}$  (evaluated at 10 MHz). After irradiation (blue spectrum) with ambient light for 3 min, the resistance increased to 603 k $\Omega$ , while the capacitance decreased to 0.94 pF. This result demonstrates the possibility to record light exposure as an irreversible modification of the impedance of the sample. While the observed changes are relatively small (due to the suboptimal matching between the polymer thickness and the microelectrodes geometry), they are very reproducible and cannot be observed if the sample is exposed to longer wavelengths, outside the absorbance range of the sensitizer, such as red light.

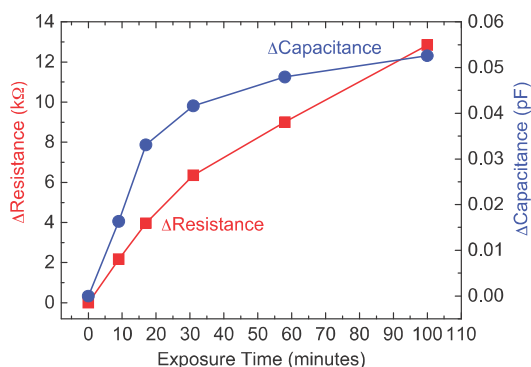


Fig. 3. Dependence of the sensor resistance  $R$  (measured at 10 kHz) and capacitance  $C$  (at 10 MHz) on the exposure time measured immediately after irradiation with a green LED (peaked at 526 nm wavelength).

Furthermore, the modification of the capacitance value cannot at all be attained on a control sample composed only of PVA (see Fig. 2(d)) or of all the components of the formulation except for the electron donor, demonstrating that the photopolymer process induces the observed changes. These changes must reflect a variation of the relative dielectric constant  $\epsilon_r$  of the photopolymer film.

### 3.2. Effect of the exposure time

The minimum exposure time required to reliably trigger the photopolymerization is around 1 min (shorter times were not investigated, being not relevant for the target application). After the initial exposure, the reaction continues also in dark, until the full conversion of the polymer layer is reached. However, in dark the polymerization is slower due to the increase of the material viscosity caused by the lack of new radicals, leading to a settling time in the order of 2 h. Nevertheless, this time is perfectly suitable for the perspective application of checking the status of the packaging of a light-sensitive good at the end of storing and transportation phases. In order to investigate the effect of an intermediate interrogation of the sensor, Fig. 3 reports the variations of  $R$  and  $C$  measured immediately after the specified exposure time (from 10 to 100 min) on a test device with the same geometry as in Fig. 2. It can be noticed that, thanks to the steepness of the initial curve slope, after only 10 min of exposure, 30% of the final capacitance variation is already obtained and, after 1 h, the steady state value has been almost completely reached ( $\sim 90\%$  for  $C$  and  $\sim 70\%$  for  $R$ ). The sensor is not intended as a light dosimeter, rather as a binary tester providing an irreversible Yes/No answer to the light exposure check. Thus, if a threshold on the impedance variation is set, then two operation scenarios can take place. If the exposure is very short (around 1 min), then the interrogation must be performed after at least 1 h. On the other hand, if the interrogation is performed shortly after exposure (less realistic case), then there is a minimum detectable exposure time, which is related to the threshold level (for instance for a 50% threshold on  $\Delta C$ , the minimum time is about 15 min).

### 3.3. Design considerations

The sensor tag consists of the combination of the modified commercial RF EAS tag with the planar interdigitated sensor. When the interdigitated sensor is connected to the tag, the simultaneous variations of  $R$  and  $C$  affect the resonance, thus offering multiple detection approaches. The decrease of  $C$  produces an increase of the resonance frequency ( $f_c \sim (LC)^{-1/2}$ ), while the increase of  $R$  increases the quality factor  $Q = R(CL)^{1/2}$ . For the readout, it is much easier to detect accurately a shift of resonance frequency  $f_c$  rather than a variation of  $Q$ , thus leading to the conclusion that the main

transduction mechanism that we should leverage in this case is capacitive.

The response to light is related to the changes in the electrical properties of the active layer which modifies the impedance of the interdigitated sensor tag. Hence the sensitivity to light will be higher where the electric field is higher, the profile of which depends on the geometry of the sensor. It is therefore important to study the sensitivity to light in the coplanar geometry (with a highly inhomogeneous vertical electric field distribution) as a function of both the gap between the fingers  $d$  and the film thickness  $t$ . Since about 90% of the fringing field lines in the vertical plane are confined within a height equal to the gap, a rule of thumb for the sizing of the device is matching  $t$  with  $d$ . More precise indications for the optimal device design are provided in the next section based on numerical simulations.

### 3.4. Extraction of the dielectric constant variation

In order to perform a quantitative analysis of the sensor impedance behavior, it is necessary to estimate the dielectric constant of the photopolymer and its variation due to light exposure in order to assess the maximum capacitance variation achievable with this material. Thus, we fabricated and used a parallel-plate vertical capacitor where a  $6 \mu\text{m}$  thick film of the active material is sandwiched between two cross-bar electrodes, the bottom one made of ITO deposited on a glass substrate and the top one made of gold deposited on top of the polymer. The average dielectric constant  $\epsilon_r$  measured for a few devices after exposure equals to  $4.4 \pm 0.3$ , which is in agreement with the literature [19] for studies on the dielectric constant of pure PVA. Unfortunately, the same measurement cannot be performed on unexposed samples (i.e. in dark, before exposure) because the evaporation of the top electrode causes the initiation of the polymerization. Consequently, coplanar electrodes (with a set of different gaps  $d = 5, 10, 20, 30$  and  $40 \mu\text{m}$ ) covered with a photopolymer film thickness  $t = 20.5 \mu\text{m}$  are employed, in combination with conformal mapping analytical expressions based on elliptic integrals for the case of a finite thin dielectric layer [23], to fit the measured resistance and capacitance values as a function of  $d$ , before and after irradiation with a 526 nm light, as reported in Fig. 4(a) and (b) respectively. The extraction of the values of capacitance is slightly complicated due to its pseudo-capacitive behavior (a constant phase element with exponent = 0.85 and phase =  $-80^\circ$ ). However, due to the narrow-band operation of the sensor, the equivalent capacitance is estimated in the frequency range of the tag resonance (i.e. around 10 MHz). As reported in Fig. 4(a), the change of the resistance upon exposure ( $\Delta R$  at 10 kHz) increases with  $d$  (with a slope of  $8.6 \text{ k}\Omega/\mu\text{m}$ ) since  $R$ , both before exposure ( $R_{\text{before}}$ ) and after ( $R_{\text{after}}$ ), increases with the distance between the fingers. Instead, the change in capacitance ( $\Delta C$  at 10 MHz) decreases with  $d$  since, by increasing the separation between the fingers, both  $C_{\text{after}}$  and  $C_{\text{before}}$  decrease. Thanks to the good fitting (Fig. 4(b)), it has been possible to extract the value of the relative dielectric constant ( $\epsilon_r$ ) in the unexposed state, corresponding to a value of 6. Thus, upon exposure to light, the normalized decrease of the photopolymer dielectric constant is  $\Delta\epsilon_r/\epsilon_r = -27\%$ . This result proves the suitability of the proposed material for this binary light-sensing purpose and sets the maximum capacitance variation achievable with this photopolymer.

Once  $\Delta\epsilon_r$  has been obtained, numerical simulations based on conformal mapping [23] can be used to optimally design the device geometry in order to maximize the impact of  $\Delta\epsilon$  variation into  $\Delta C$  variation. For instance, Fig. 4(c) shows the normalized capacitance variation ( $\Delta C/C$ ) as a function of the film thickness for the same inter-electrode gap ( $5 \mu\text{m}$ ) of the test device. It can be observed

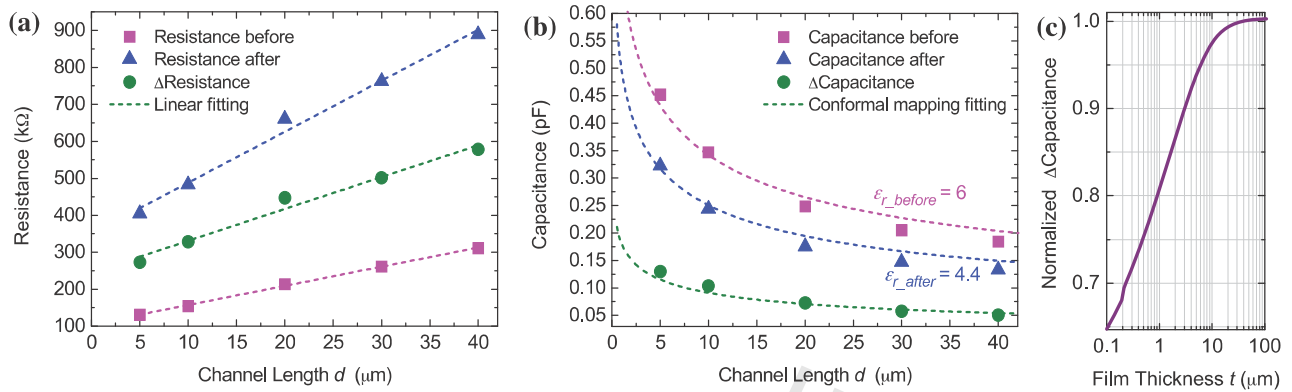


**Fig. 4.** Systematic investigation of the sensor impedance dependence on the major design parameter: the finger distance  $d$ . Measured capacitance values (b) were fitted with conformal mapping expressions for a thin ( $t = 20.5 \mu\text{m}$ ) finite dielectric layer, allowing the extraction of the value of the dielectric constant of the polymer in the initial dark state  $\epsilon_r = 6$ , corresponding to  $\Delta\epsilon_r/\epsilon_r = -27\%$ . (c) Numerical simulation of the normalized capacitance variation as a function of  $t$  for  $d = 5 \mu\text{m}$ .

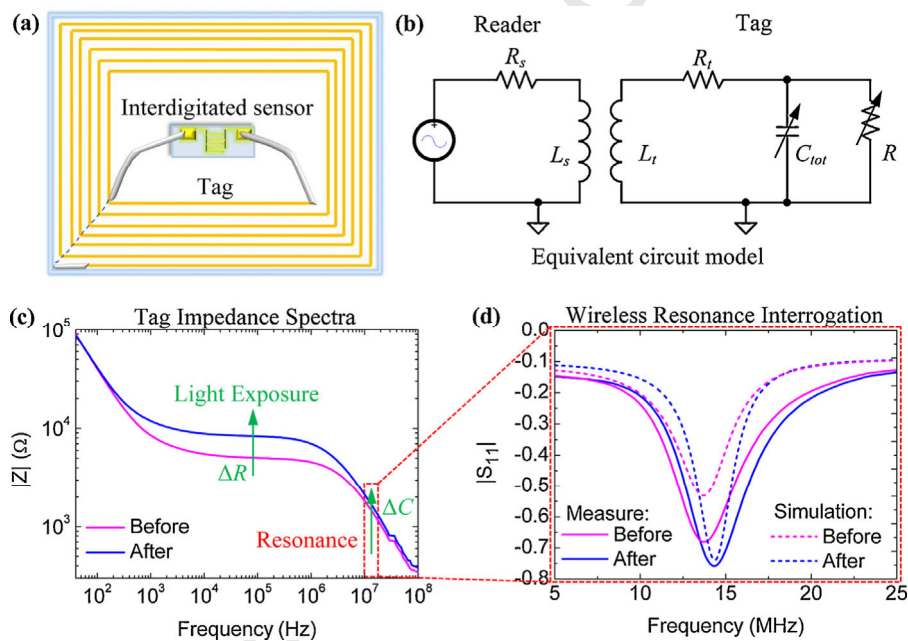


**Fig. 5.** Characterization of the complete sensor embedded in the tag (a). Equivalent impedance model (b) and directly measured impedance spectra (c) were used to confirm with circuit simulations the observed resonance shift (d) toward a higher frequency (by 540 kHz) after exposure of the tag to light.

that, above a polymer thickness of  $20 \mu\text{m}$ , the curve is flat and  $\Delta C/C$  saturates, indicating that the maximum variation is obtained.

### 3.5. Complete photosensitive chipless tag

Based on the analysis discussed in the previous section, the final dimensions of the interdigitated sensor embedded in the tag (Fig. 5(a)) are:  $d = 5 \mu\text{m}$ ,  $t = 98 \mu\text{m}$  (largely exceeding  $20 \mu\text{m}$ ) and  $\ell = 2.5 \text{ cm}$ . The response of the complete device is probed in non-contact mode, by means of a loop antenna directly connected to a network analyzer. The complete electrical equivalent model is shown in Fig. 5(b): the transformer models the inductive coupling between the reader coil and the tag coil, while  $C_{tot}$  includes both the tag capacitance and the sensor capacitance that are in parallel. The Bode plots of the impedance spectra of this sensor before and after exposure are reported in Fig. 5(c). The impedance of the tag alone had been previously measured, thus obtaining the value of the inductance  $L_t = 14.5 \pm 0.1 \mu\text{H}$  and a stray series resistance  $R_t = 30 \Omega$ . The values of the parameters extracted from the impedance spectra directly measured at the resonator terminals are reported in

Table 1. As shown in Fig. 5(d), the  $S_{11}$  parameter measured with the contact-less reader clearly demonstrates the shift of the resonance frequency, increasing from 13.8 MHz to 14.4 MHz after exposure to light (for 1 min and measured after 5 h to prove the non-volatility of the recording of the event). Furthermore, the experimental resonance curves (and in particular the position of  $f_c$ ) are consistent with PSpice simulations (dashed lines) of the equivalent circuit performed with the parameters reported Table 1.

A capacitance change of 7% (corresponding to a 4% increase of the resonance frequency) may appear a small shift, starting from a 27% variation of the photopolymer dielectric constant. It

**Table 1**

Summary of the electrical parameters of the RFID light sensitive tag before and after photo-induced polymerization process (ambient light, exposure time 1 min, read after 5 h).

Condition	$C_{tot}$ (pF)	$R$ (kΩ)	$f_c$ (MHz)	$Q$
Before	9.14	5	13.82	2.64
After	8.47	8.4	14.36	2.87
Variation (%)	-7.33	68	4	8

is worth noting that this is mainly due to the fact that the fixed capacitance of the commercial tag ( $\sim 4.5$  pF) and the interdigitated sensor capacitance in parallel to it have comparable values. Furthermore, the latter is changing only by a factor  $27\%/2$  since only the upper electric field lines of the sensor are immersed in the photopolymer, while the bottom lines are immersed in the substrate which remains constant. An engineered design, comprising a custom coil with reduced stray capacitance and an increased sensor capacitance, can effectively enhance the resonance frequency modification with respect to the proof-of-concept demonstrated here. In any case, the measured variation corresponds already to a shift of 540 kHz that is of the same order of magnitude of what has been achieved for all-printed sensors [24]. Furthermore and most importantly, this shift is compatible with the detection resolution of commercial 13.56 MHz RFID readers such as the integrated transceiver MLX90121 by Melexis that in FSK (Frequency Shift Keying) mode provides a selectable demodulation bandwidth between 200 and 1400 kHz. Of course, if this proof-of-concept implementation were used without further improvement, it would be necessary to measure the resonance frequency in dark (with an accuracy better than 4%) and store this value for each single tag, for differential comparison during the following tag interrogations.

When looking at the field operation of the sensor, one of the most critical aspects, common to all the devices of the broad family of the chemo-physical resonating passive sensors, is the sensitivity of all the electrical parameters to temperature (and humidity) variations. Among classical approaches such as the introduction of a thermal sensor for calibration or the addition of a non-functionalized dummy sensor as a reference for differential sensing, an interesting solution has been proposed especially for this class of sensors. It has been demonstrated that by leveraging the different temperature dependences of each electrical parameter, it is possible to perform multivariate analysis and achieve, through principal component analysis, self-correction against thermal fluctuations [25].

#### 4. Conclusions

In this work we have proposed a simple approach to develop novel wireless sensors, namely photosensitive chipless RF tags based on the coupling of a standard LC resonator and of an optimized planar interdigitated sensor covered by an acrylamide photopolymer film acting as an irreversible light sensor. The exposure to visible light triggers the polymerization, which modifies the electrical properties of the film (decreasing its dielectric constant by 27%) and, as a consequence, the complex impedance of the sensor embedded in the tag. We have demonstrated that 1 min exposure to ambient light (500–550 nm) produces an irreversible and stable shift of the tag resonance frequency (+540 kHz) that is detectable by commercial 13 MHz RFID readers.

Such a single-bit sensor is very simple and robust, and its fabrication is compatible with high-throughput printing processes, therefore drastically reducing the cost per tag. Consequently, these disposable wireless sensors can be used to tag goods in large volumes that need to be stored and transported in dark conditions (such as food or pharmaceutical products) or under specific illumination conditions. If the good is accidentally exposed to a forbidden light source, this event can be verified wirelessly, even by means of ubiquitous smartphones endowed with NFC (Near-Field Communication) capabilities [26], at any time and very quickly by looking at the irreversible shift of the resonance frequency, without interfering with the original sealed packaging. Furthermore, when the present laboratory-scale and mostly manual fabrication process will be consolidated into an industry-scale process, the antenna coil and the interdigitated electrodes will be patterned together and

further optimized by increasing the area of the sensor (while keeping the same  $f_c$ ) in order to reduce the sensitivity to stray effects and maximize the signal variation.

#### Acknowledgements

The authors are thankful to Marco Consani for inspiring discussions and support at the initial stage of the research. This work was partially supported by Fondazione Cariplo through the project “S2N”, grant no. 2010-1351.

#### References

- [1] K. Finkenzeller, RFID Handbook, 2nd ed., John Wiley & Sons, 2003.
- [2] E.M. Amin, N.C. Karmakar, Development of a low cost printable humidity sensor for chipless RFID technology, in: Proc. IEEE RDIF Conf., 2012.
- [3] S. Preradovic, N.C. Karmakar, Chipless RFID tag with integrated sensor, IEEE Sens. J. (2010) 1277–1281.
- [4] A.N. Nambiar, RFID technology: a review of its applications, Lect. Notes Eng. Comp. (2009) 1253–1259.
- [5] S. Preradovic, N.C. Karmakar, Chipless RFID Tag in Multiresonator-Based Chipless RFID, Springer, 2012, pp. 77–94.
- [6] J.J. Ryan, Anti shoplifting labels, Sci. Am. 5 (1977) 120–125.
- [7] M.A. Fonseca, J.M. English, M. von Arx, M.G. Allen, Wireless micromachined ceramic pressure sensor for high-temperature applications, IEEE Conf. Microelectromech. Syst. 11 (2002) 337–343.
- [8] C. Occhiuzzi, A. Rida, G. Marrocco, M. Tentzeris, RFID passive gas sensor integrating carbon nanotubes, IEEE Trans. Microw. Theory 59 (2011) 2674–2684.
- [9] L. Yang, R.W. Zhang, D. Staiculescu, C.P. Wong, M.M. Tentzeris, A novel conformal RFID-enabled module utilizing inkjet-printed antennas and carbon nanotubes for gas-detection applications, IEEE Antenna Wirel. Propag. Lett. 8 (2009) 653–656.
- [10] M.V. Kulkarni, S.K. Apte, S.D. Naik, J.D. Ambekar, B.B. Kale, Ink-jet printed conducting polyaniline based flexible humidity sensor, Sens. Actuators B 178 (2013) 140–143.
- [11] T.J. Harpster, B. Stark, K. Najafi, A passive wireless integrated humidity sensor, Sens. Actuators A 95 (2002) 100–107.
- [12] D.A. Sanz, E.A. Unigarro, J.F. Osma, F. Segura-Quijano, Low cost wireless passive microsensors for the detection of hazardous compounds in water systems for control and monitoring, Sens. Actuators B 178 (2013) 26–33.
- [13] M.S. Mannoor, H. Tao, J.D. Clayton, A. Sengupta, D.L. Kaplan, R.R. Naik, et al., Graphene-based wireless bacteria detection on tooth enamel, Nat. Commun. 3 (2012).
- [14] J. Garcia-Canton, A. Merlos, A. Baldi, High-quality factor electrolyte insulator silicon capacitor for wireless chemical sensing, IEEE Electron Device Lett. 28 (2007) 27–29.
- [15] Z.A. Strong, A.W. Wang, C.F. McConaghy, Hydrogel-actuated capacitive transducer for wireless biosensors, Biomed. Microdevices 4 (2002) 97–103.
- [16] B.E. Horton, S. Schweitzer, A.J. DeRouin, K.G. Ong, A varactor-based, inductively coupled wireless pH sensor, IEEE Sens. J. 11 (2011) 1061–1066.
- [17] K.M. Shungo Sugawara, T. Kitayama, Holographic recording by dye-sensitized photopolymerization of acrylamide, Appl. Opt. 14 (1975) 378–382.
- [18] J.R. Lawrence, F.T. O'Neill, J.T. Sheridan, Photopolymer holographic recording material, Optik 112 (2001) 449–463.
- [19] J.P. Fouassier, F. Morlet-Savary, J. Lalevée, X. Allonas, C. Ley, Dyes as photoinitiators or photosensitizers of polymerization reactions, Materials 3 (2010) 5130–5142.
- [20] C. Meka, R. Jallapuram, I. Naydenova, S. Martin, V. Toal, Development of a panchromatic acrylamide-based photopolymer for multicolor reflection holography, Appl. Opt. 49 (2010) 1400–1405.
- [21] S. Heun, M. Borsenberger, Hole transport in triethylamine doped polymers, Physica B: Condens. Matter 216 (1995) 43–52.
- [22] G. Joshi, S.M. Pawde, Effect of molecular weight on dielectric properties of polyvinyl alcohol films, J. Appl. Polym. Sci. 102 (2006) 1014–1026.
- [23] R. Igreja, C.J. Dias, Analytical evaluation of the interdigital electrodes capacitance for a multi-layered structure, Sens. Actuators A 112 (2004) 291–301.
- [24] X. Wang, O. Larsson, D. Platt, S. Nordlinder, I. Engquist, M. Berggren, X. Crispin, An all-printed wireless humidity sensor label, Sens. Actuators B 166–167 (2012) 556–561.
- [25] R.A. Potyrailo, C. Surman, A passive radio-frequency identification (RFID) gas sensor with self-correction against fluctuations of ambient temperature, Sens. Actuators B 185 (2013) 587–593.
- [26] J.M. Azzarelli, K.A. Mirica, J.B. Ravnsbæk, T.M. Swager, Wireless gas detection with a smartphone via RF communication, PNAS 111 (2014) 18162–18166.

## Biographies

**Malena Oliveros** obtained her Ph.D. degree in 2011 in Materials Science from the University of Autònoma de Barcelona (Spain). From 2011 to 2013 she was a post-doctoral fellow at the Politecnico di Milano, Physics Department, and collaborated with the Center for Nano Science and Technology @PoliMi (Milan, Italy) of the Istituto Italiano di Tecnologia (IIT). She is currently a postdoctoral researcher at the headquarters of IIT in Genoa (Italy). Her research focuses in multifunctional materials and their applications: thermal, high voltage and high mechanical resistance composites.

**Marco Carminati** born in 1981, received B.Sc. and M.Sc. in Electronic Engineering, both cum laude from the Politecnico di Milano (Italy), in 2003 and 2005, respectively. In 2008 was awarded a Rocca Fellowship and spent a semester at MIT working on BioMEMS. In 2009 he completed his Ph.D. in Electronics and Information Science at DEIB, Politecnico di Milano where he is currently a post-doctoral fellow designing and developing high-sensitivity impedance sensors and low-noise instrumentation for nano-bio-science. He has authored more than 60 peer-reviewed international publications and holds one patent.

**Alessio Zanutta** is a research fellow at the INAF– Astronomical Observatory of Brera. He obtained his Ph.D. degree in 2015 in Materials Engineering from the Politecnico di Milano (Italy). During his doctorate he collaborated with the INAF developing new materials for holographic optical dispersive elements to be used in astronomy.

**Tommi Mattila** has worked since 1999 at VTT Technical Research Centre of Finland. His expertise areas cover wireless systems and RF technology, sensors, flexible and hybrid electronics, and microelectromechanics. At the moment, he works as the Chief Technology Officer for Posterfy Ltd. (a spin-off company of VTT).

**Salme Jussila** received Ph.Lic. degree (1996) and M.Sc. degree (1985) in physics from University of Helsinki. Before graduation in 1985 he worked for one year as a research trainee in Electron Physics laboratory of Helsinki University of Technology. He worked as a research scientist at VTT Technical Research Centre of Finland during 1985–2013 in the research team, which was responsible for the development of organic electronics and conducting polymers.

**Kaj Nummila** born in 1960 in Salo (Finland), attained a Doctor degree from Helsinki University of Technology (HUT) in 1989. Dr. Nummila acted as manager of the nuclear magnetism research group at Low Temperature Laboratory (LTL) at HUT. Dr. Nummila has a doctor degree at HUT in physics since 1996. After joining VTT, Technical Research Centre of Finland in 1998 he has worked as group manager and as a principal scientist mainly developing electromagnetic, RF- and microwave sensors for industrial use. During the last ten years he has been developing radiofrequency identification (RFID) systems, wireless sensors and industrial measurement solutions.

**Andrea Bianco** is a researcher at the INAF-Osservatorio Astronomico di Brera. In 2004, he got a PhD in materials Engineering at Politecnico di Milano working on the application of organic functional materials in astronomical instrumentation. From 2005 to 2010 he was a tenure track researcher at the INAF-Osservatorio Astronomico di Brera, then he got a permanent position in the same institution. His research interests focus on the design and development of holographic optical elements for astronomical instrumentation and the application of photochromic materials in adaptable refractive and diffractive optical elements.

**Guglielmo Lanzani** is head of the Center for Nano Science and Technology @PoliMi of the Istituto Italiano di Tecnologia, and full professor in physics at Politecnico di Milano. His research regards the photophysics of conjugated carbon materials (organic semiconductors, polyconjugated compounds and carbon nanotubes) and nanostructures, including devices and applications, as reported in more than 220 papers. Leading activities are on solar energy conversion and bio organic interfaces.

**Mario Caironi** is a Tenure Track Researcher at the Center for Nano Science and Technology @PoliMi (Milan, Italy) of the Istituto Italiano di Tecnologia (IIT). He obtained his Ph.D. in 2007 at Politecnico di Milano and then joined Prof. Sirringhaus' group at the Cavendish Laboratory (Cambridge, UK) to work on inkjet-printed, downscaled organic field-effect transistors (OFETs). He moved to IIT in 2010 as a Team Leader, and was recipient of a Career Integration Grant Marie-Curie project to work on Inkjet-Printed organic Photodetectors for Imaging Applications. He is an ERC 2014 grantee.